

# Machine learning for percolation utilizing auxiliary Ising variables

Junyin Zhang,<sup>1,\*</sup> Bo Zhang,<sup>1,\*</sup> Junyi Xu,<sup>2</sup> Wanzhou Zhang,<sup>3,2,†</sup> and Youjin Deng<sup>1,4,5,‡</sup>

<sup>1</sup>*Hefei National Laboratory for Physical Sciences at the Microscale and Department of Modern Physics,  
University of Science and Technology of China, Hefei 230026, China*

<sup>2</sup>*College of Physics and Optoelectronics, Taiyuan University of Technology, Shanxi 030024, China*

<sup>3</sup>*CAS Key Laboratory of Quantum Information, University of Science and Technology of China*

<sup>4</sup>*Shanghai Research Center for Quantum Sciences, Shanghai 201315, China*

<sup>5</sup>*MinJiang Collaborative Center for Theoretical Physics,*

*College of Physics and Electronic Information Engineering, Minjiang University, Fuzhou 350108, China*

(Dated: October 14, 2021)

Machine learning for phase transition has received intensive research interest in recent years. However, its application in percolation still remains challenging. We propose an auxiliary Ising mapping method for machine learning study of the standard percolation as well as a variety of statistical mechanical systems in correlated percolation representations. We demonstrate that unsupervised machine learning is able to accurately locate the percolation threshold, independent of the spatial dimension of system or the type of phase transition, which can be first order or continuous. Moreover, we show that, by neural network machine learning, auxiliary Ising configurations for different universalities can be classified with high confidence level. Our results indicate that the auxiliary Ising mapping method, despite of its simplicity, can advance the application of machine learning in statistical and condensed-matter physics.

## I. INTRODUCTION

The percolation model was first proposed as a model for a porous medium by Broadbent and Hammersley in 1957 [1] and then has been applied in physics, materials science, epidemiology, finance and other fields [2–5]. As a paradigm of random and semi-random connectivity, percolation models on regular lattices or complex network have played a key role in the statistical mechanics and network science [6–9]. Standard percolation is defined as the random and independent occupation of each site or bond on a lattice or complex network according to a certain probability. Furthermore, correlated percolation is also proposed [10–14] to capture the thermal properties of various physical models, in which the occupation probability of each site or bond is not independent. The concept of correlated percolation is used later in the famous Swendsen-Wang algorithm [15].

Recently, machine learning has provided new ideas and methods for studying various physical problems [16], among which the phase transition is one of the fruitful topics. Machine learning can generally be divided into supervised and unsupervised learning. Besides the extensive works by supervised phase detection, many studies based on unsupervised phase detection have also been reported recently, such as the principal component analysis (PCA) [17–19], the t-Distributed Stochastic Neighbor Embedding (t-SNE) [20–22], the diffusion map [23–26] and the confusion scheme [27] *et al.* However, it is still a challenge for unsupervised machine learning to detect the percolation phase transition points properly [20, 28, 29].

Ref. [28] pointed out that, after reducing the dimensionality of the original configuration using the PCA method, no statistically significant correlations can be found between the principal components and the ordinal parameters. As far as the confusion method, Ref. [29] found that the performance curve appeared to have a V-shape instead of a W-shape. Regarding the t-SNE method, it also fails to learn the phase transition of the percolation model, although it can clearly separate the configurations far away from the percolation threshold [20].

The difficulty in applying machine learning methods to percolation models lies in two parts. On the one hand, the lattice (graph) structures play a crucial role in the percolation model and must be encoded in the training set, otherwise the critical behaviors of the percolation models can never be captured; on the other hand, percolation is a global property which is difficult to be captured. For similar reasons, the unsupervised phase detection on the XY model is only possible when the data is pre-classified by different global winding numbers [23, 30].

Motivated by the previous research works [20, 28, 29], in this paper, we propose the auxiliary Ising mapping (AIM) method, which maps the original percolation configuration into an Ising-like spin configuration. The AIM method preserves all correlation functions unchanged and captures the network structure. After such a mapping, we apply the confusion scheme to the spin configurations and find that the percolation phase transition can be detected in an unsupervised way, as shown in Fig. 1. Beyond the uncorrelated percolation model, we successfully extract the thermal phase transitions of the Potts models and obtain a similar result as Refs. [31, 32] for the XY model in the representation of correlated percolation clusters. Our method is generally applicable to any other model as long as it can be formulated in the framework

\* These two authors contributed equally to this paper.

† Corresponding author: zhangwanzhou@tyut.edu.cn

‡ Corresponding author: yjdeng@ustc.edu.cn

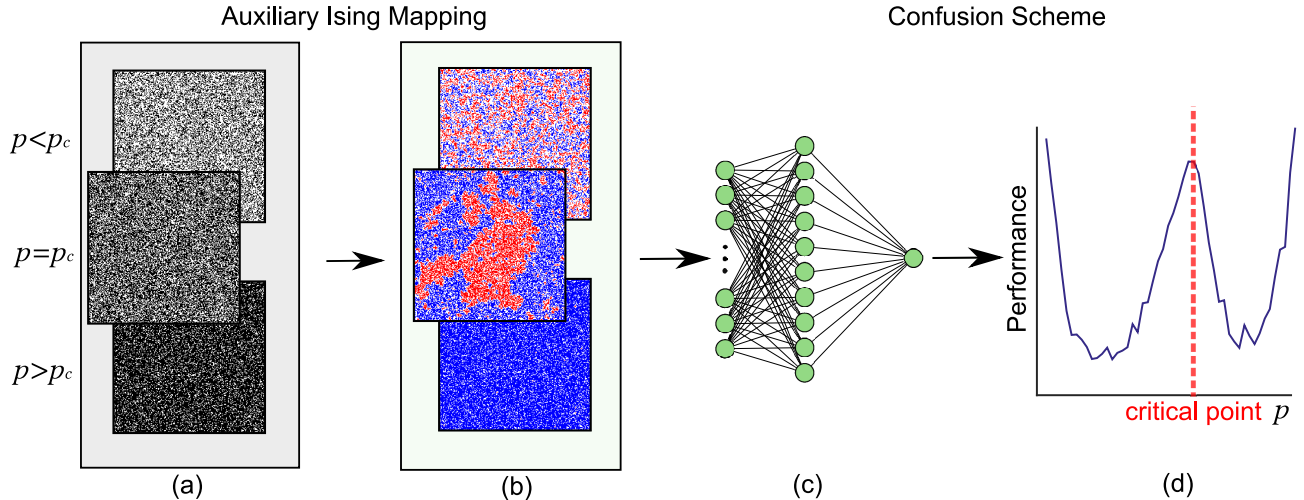


FIG. 1. The main idea of this work. Auxiliary Ising mapping (AIM) is introduced to transform the original percolation configuration into an Ising-like spin configuration, while all the correlation functions are kept unchanged. After applying the AIM, the percolation phase transition can be identified in an unsupervised way using a confusion scheme based on the neural network, the details of the network are in the Appendix A 1. (a) The three snapshots from top to bottom are the original configurations (in black and white colors) of the site percolation on the square lattices with occupation probabilities  $p = 0.4$ ,  $0.593$  (the percolation threshold) and  $0.8$ , respectively. (b) The corresponding configurations obtained after AIM. The auxiliary Ising spins are colored in blue and red, and the unoccupied sites are colored in white. The percolation clusters emerged as the  $p$  increases. (c) The fully connected neural network, including one input layer, one hidden layer, and one output neuron, works as a binary classification neural network. (d) The W-shaped confusion performance curve with the central peak locates at the percolation threshold indicates the percolation transition.

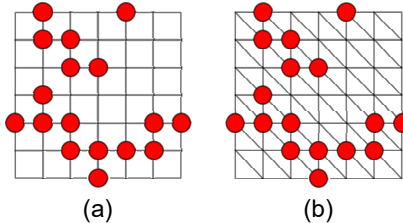


FIG. 2. The occupation configurations on (a) the square and (b) the triangular lattices for the site percolation models. Occupied and non-occupied sites are indicated by red symbols and empty sites, respectively. For these two configurations, if only the occupancy configurations are fed in, the neural network can never learn the differences between the different lattices (graphs) and therefore will never learn percolation transition correctly.

of percolation.

The present paper is organized as follows: Sec. II introduces the AIM method and successfully applies it to the percolation models on various lattices and complex networks. Then, we promote our method to learn the phase transitions of the generalized percolation model like the Potts model and the XY model. Sec. III demonstrates that the configurations of the different models at the phase transition point could be classified by the neural network after the AIM transformation. Sec. IV is the summary and future perspective.

## II. PERCOLATION TRANSITION DETECTION

Identifying phase transitions in a site percolation model through unsupervised machine learning is a challenge [20, 28, 29]. The problem lies mainly in how to feed the lattice structure of the percolation model as information into the neural networks and other machine learning tools. Suppose we only input the occupation configurations (as in Refs. [20, 28, 29]) into the neural network, the structure information of the lattice is largely discarded, and the network is unlikely to identify the difference between percolation models in different lattices in an unsupervised way, as illustrated in Fig. 2. This difficulty can be solved by the AIM method that introduced below, in which the structure information of the lattice and the occupation configurations are combined.

### A. Auxiliary Ising Mapping

To generate a site percolation configuration with occupation probability  $p$ , the standard procedure is to visit each lattice site sequentially, draw a uniform random number  $\text{rand}() \in [0, 1]$ , and assign to the site a variable  $s = 1$  if  $\text{rand}() < p$  and otherwise,  $s = 0$ . The AIM method extends the variable from  $s \in \{0, 1\}$  to  $\{0, \pm 1\}$  and generates a site percolation configuration in an epidemic-spreading way. All the whole sites are initialized to be nonvisited, and, by sequentially visiting the

lattice, the first occupied site, called the seed site, is infected by diseases  $s = \pm 1$  with equal probability. The seed site then spreads its disease to each of the neighboring and unvisited sites with probability  $p$ . Note that a visited site, no matter it is empty or already sick, can no longer be infected by the disease. The epidemic keeps spreading until all its boundary sites are visited, and a cluster of infected sites with disease  $s = +1$  or  $-1$  is formed. Afterward, one sequentially visits the remaining unvisited sites until the next seed site is obtained. The procedure is repeated till all the lattice sites are visited. A configuration of dilute Ising variables  $\{s = 0, \pm 1\}$  is generated, as shown in Fig. 3.

The above algorithm ensures that the correlation function  $G$  remains unchanged between the percolation and the AIM spin configurations. For a given lattice (graph) structure and the occupation probability  $p$ , several percolation configurations  $\{\mathcal{C}\}$  can be generated. The correlation function  $G(\vec{r}_i, \vec{r}_j)$  refers to a probability that two sites at locations  $\vec{r}_i$  and  $\vec{r}_j$  belong to the same cluster and is defined as the following:

$$G(\vec{r}_i, \vec{r}_j) = \langle \Theta(\mathcal{C}; \vec{r}_i, \vec{r}_j) \rangle_{\mathcal{C}}, \quad (1)$$

where the correlation index defined for one specific configuration  $\mathcal{C}$  is:

$$\Theta(\mathcal{C}; \vec{r}_i, \vec{r}_j) = \begin{cases} 0, & \vec{r}_i, \vec{r}_j \text{ in different clusters} \\ 1, & \vec{r}_i, \vec{r}_j \text{ in the same clusters} \end{cases}. \quad (2)$$

The  $\langle \dots \rangle_{\mathcal{C}}$  refers to the average of all occupation configurations according to statistical weights. If  $N_C$  clusters exist in the configuration  $\mathcal{C}$ , then there are  $2^{N_C}$  different methods to map it into various auxiliary Ising configurations. A specific auxiliary Ising mapping  $AIM_{\alpha}$  is defined by the Ising spins specified on the  $N_c$  clusters  $\alpha : \{\tilde{s}_1, \dots, \tilde{s}_{N_C}\}$ . Different mappings can be labeled as

$$AIM_{\alpha} : \quad \mathcal{C} \xrightarrow{\alpha} \mathcal{S}, \quad (3)$$

and they lead to various spin configurations  $\mathcal{S}$  on a lattice with  $N$  sites, i.e.,  $\{s_1, \dots, s_N\}$ , by which the correlation between two spins  $\langle s_i s_j \rangle_{\alpha}$  still equals to  $\Theta(\mathcal{C}; \vec{r}_i, \vec{r}_j)$ . This can be understood in the following way. If the sites at  $\vec{r}_i$  and  $\vec{r}_j$  belong to the different clusters, then the correlation satisfy the relation  $\langle s_i s_j \rangle_{\alpha} = \langle s_i \rangle_{\alpha} \langle s_j \rangle_{\alpha} = 0$  because the different components of  $\{\tilde{s}_1, \dots, \tilde{s}_{N_C}\}$  are independent from each other. If the sites at  $\vec{r}_i$  and  $\vec{r}_j$  belong to the the same cluster, then the correlation  $s_i s_j = (\pm 1)^2 = 1$  always holds.

Therefore, averaging over various percolation configurations  $\mathcal{C}$  and mappings  $\alpha$ , the two-point correlation functions of the percolation and spin models are equivalent and can be expressed as follows

$$G(\vec{r}_i, \vec{r}_j) = \langle \Theta(\mathcal{C}; \vec{r}_i, \vec{r}_j) \rangle_{\mathcal{C}} = \langle \langle s_i s_j \rangle_{\alpha} \rangle_{\mathcal{C}} = \langle s_i s_j \rangle_{\mathcal{S}}. \quad (4)$$

In addition to correlation itself, the AIM algorithm preserves all physical quantities that can be expressed

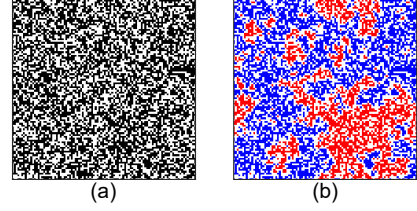


FIG. 3. The auxiliary Ising mapping for the square-lattice site percolation. (a) In the initial percolation configuration, occupied sites are marked black, while unoccupied sites are marked white. (b) The AIM configuration. These clusters by the occupied sites are randomly labeled  $+1$  and  $-1$  according to a probability of  $1/2$ .

as correlation function and the critical behavior of the percolation model. As an example, we show that the second-order moment of the cluster size  $S_2 = \langle \sum_k C_k^2 \rangle_{\alpha} / N$  is equal to the susceptibility  $\chi = \langle M^2 \rangle_{\alpha} / N$  of the AIM configurations, where  $C_k$  refers to the size of the  $k$ -th cluster and  $N$  represents the total sites on the system. Using this relationship, the susceptibility, which has a divergent behavior characterized by the magnetic exponents near the critical point, remains unchanged using the AIM method.

To prove  $\chi = S_2$ , one can express the magnetization for the AIM configurations as,

$$M = \sum_{i=1}^N s_i = \sum_{k=1}^{N_C} C_k \tilde{s}_k, \quad (5)$$

where  $\tilde{s}_k$  is the spin status ( $\pm 1$ ) of the  $k$ -th cluster. Then, the squared magnetization reads

$$\begin{aligned} \langle M^2 \rangle_{\alpha} &= \langle \sum_k \sum_{k'} C_k C_{k'} \tilde{s}_k \tilde{s}_{k'} \rangle_{\alpha} \\ &= \langle \sum_k C_k^2 \tilde{s}_k^2 \rangle_{\alpha} + \langle \sum_k \sum_{k' \neq k} C_k C_{k'} \tilde{s}_k \tilde{s}_{k'} \rangle_{\alpha} \\ &= \langle \sum_k C_k^2 \rangle_{\alpha}. \end{aligned}$$

During the derivation,  $\langle \sum_k \sum_{k' \neq k} C_k C_{k'} \tilde{s}_k \tilde{s}_{k'} \rangle_{\alpha} = 0$ , is used because the auxiliary Ising spins on different clusters are specified independently. The above derivation based on the site percolation models is independent of spatial dimension and lattice (graph) structures. It can be readily generalized to the bond percolation models by only changing the way to form percolation clusters, which should be based on bond connection.

## B. Learning performance of the percolation model

We classify the original configurations of the percolation and the AIM configurations using the confusion

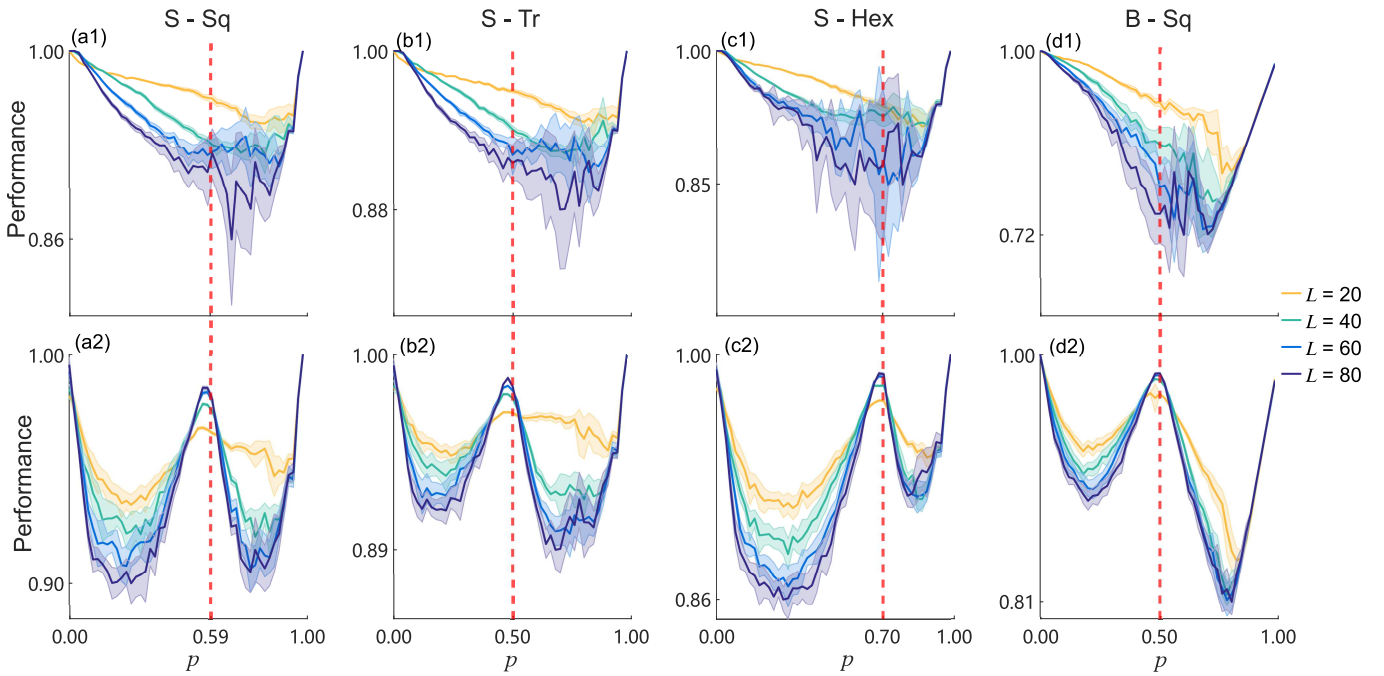


FIG. 4. The confusion performance curve for site and bond percolation models. The shaded area denotes the  $3\sigma$  errorbar. The curves with (a1-d1) original occupation configurations and (a2-d2) the configurations after AIM on (a) the square-lattice site percolation (S-Sq), (b) the triangular-lattice site percolation (S-Tr), (c) the hexagonal-lattice site percolation (S-Hex) and (d) the square-lattice bond percolation (B-Sq). The red dashed line denotes the percolation threshold. For the square lattice and triangular lattice, the number of sites  $N$  is related to linear size  $L$  by  $N = L^2$ , and for the hexagonal lattice it is  $N = 2L^2$ . All lattices come with periodic boundary conditions.

scheme. The main idea of confusion scheme is to deliberately mark the samples with trial labels, and train the classification neural network based on those trial labels, the phase transition can be identified by comparing the classification accuracy on different label sets. Details of the confusion scheme and the network structure used in our training can be found in the Appendix B.

In Fig. 4, we compare the performance curves with and without using AIM for site percolation model on the square lattice, triangular lattice, hexagonal lattice, and the bond percolation model on the square lattice. A clear difference can be seen between the performance curves of the original percolation configurations in the upper row and of the AIM configurations in the lower row, respectively. In all the four percolation models, the performance curves of the original configurations are V-shaped, which means that the neural network fails to detect any phase transition features [27]. However, clear W-shaped performance curves emerge for all neural networks trained by the AIM configurations, which indicates that the neural networks determine phase transition in an unsupervised way from the data.

To verify that the detected phase transition is exactly the percolation transition, we compare the peak position of the W-shaped performance curve and the corresponding percolation threshold for the model. In Fig. 4(a2), the peak locates at the percolation threshold for the square-lattice site percolation  $p_c = 0.59274605079210(2)$  [33, 34]

within one discrete unit  $\Delta p = 0.02$ . This is also true for the site percolation models on the triangular lattices with  $p_c = 1/2$  [35], the hexagonal lattices with  $p_c = 0.697040230(5)$  [34, 36] and the bond percolation model on the square lattices with  $p_c = 1/2$  [37], as shown in Figs. 4 (b2)-(d2), respectively. We further train the neural networks in the confusion scheme using data generated in different sizes  $L \times L$ . The results in Fig. 4 show that the peak position converges to the percolation threshold as the size increases. Since the peak position converges to the percolation threshold, we conclude that the phase transition detected by the confusion scheme from the auxiliary Ising spin configuration is exactly the percolation transition.

We further demonstrate that the percolation transition on more complex network structures can be detected in an unsupervised way after auxiliary Ising mapping. Figure 5 shows the performance curve obtained by training the network using auxiliary Ising spin configuration on (a) the site percolation on the square lattice with nearest and next-nearest-neighbouring bonds and (b) the bond percolation on the Erdős–Rényi (ER) network [38]. A clear W-shape can be seen on the performance curves, and the peaks also locate near the thresholds 0.407(2) [39, 40] and 1/2 [38] respectively. The detailed definition of ER network can be found in Appendix C.

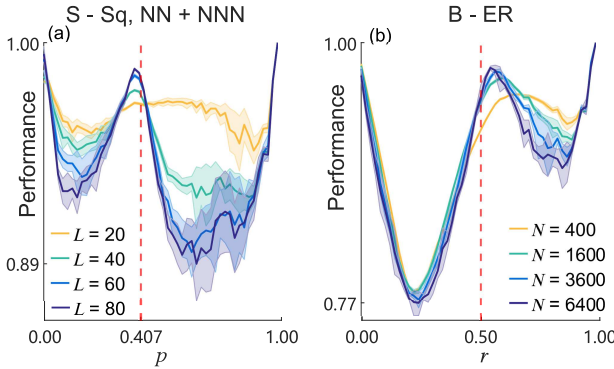


FIG. 5. The confusion performance curve for percolation on graphs. The shaded area denotes the  $3\sigma$  errorbar. The curve of (a) the site percolation on the square lattice with nearest and next-nearest-neighbouring bonds (S-Sq, NN+NNN). (b) ER Network bond percolation (B-ER), and the graphs have  $N$  nodes and  $rN$  edges. The square lattice used in (a) has a periodic boundary condition.

### C. Correlated percolation: the Potts and XY models

In this section, we study the correlated percolation transition in the Potts model and the XY model using the AIM method.

The Hamiltonians of both models are:

$$\begin{cases} H_{Potts} = -J \sum_{\langle i,j \rangle} \delta_{\sigma_i, \sigma_j} \\ H_{XY} = -J \sum_{\langle i,j \rangle} \vec{S}_i \cdot \vec{S}_j \end{cases}, \quad (6)$$

where the Potts variable takes values  $\sigma = 1, 2, \dots, q$  and the XY spin  $\vec{s}_i$  is unit vector with two real components. For both models, the ferromagnetic coupling strength is fixed with  $J > 0$  and the summation is performed over nearest-neighbor pairs  $\langle i, j \rangle$  of sites. Both of the Potts model [41–43] and the XY model [20, 23, 30–32] have been studied using machine learning methods extensively.

The Potts model can be seen as a correlated percolation model in the Fortuin-Kasteleyn (FK) representation, which is generated by connecting the nearest neighbors with the probability  $p_{ij} = 1 - e^{-\beta J \delta_{\sigma_i, \sigma_j}}$  [10]. The inverse temperature  $\beta$  is defined as  $\beta = 1/T$ . It is shown that the correlation function of the corresponding correlated percolation model is proportional to the correlation function in the original Potts model with a fixed coefficient depending on  $q$ , due to the similarity of the mapped partition functions [10]. Because of the clear dependency of the correlation function and the critical behavior, such proportionality directly results in an unchanged phase critical behavior, which maps the thermal phase transition of the Potts model into the percolation transition in the FK representation [10].

A similar correlated percolation model existed in the FK representation after being projected in one chosen di-

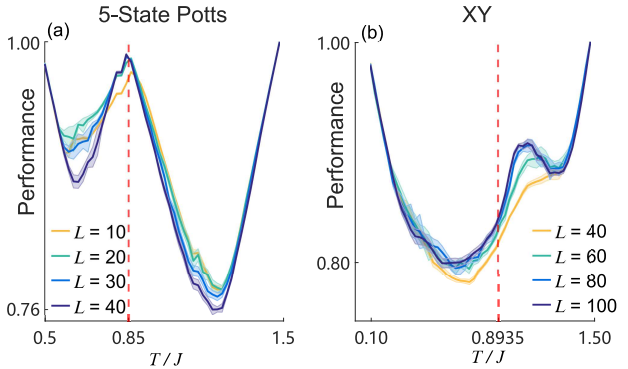


FIG. 6. The confusion performance curves for generalized percolation. The shaded area denotes the  $3\sigma$  errorbar. The curves of the (a)  $q = 5$  Potts model and (b) the XY model. The red line denotes the percolation threshold. All lattices come with periodic boundary conditions.

rection for the XY model [44]. The projected XY model can be obtained by choosing a randomly oriented Cartesian frame of reference  $(x, y)$  in the spin space and projecting all spins along the  $x$  and  $y$  axes:  $\vec{S}_i = s_i^x \hat{x} + s_i^y \hat{y}$ . The XY model then turns out to be two Ising-like models:  $H_{XY} = H_x + H_y$ . In one Ising-like projected XY model, such as that one projected on  $\hat{x}$ , the correlated percolation model in the FK representation can be built by connecting nearest sites with the probability  $p_{ij} = \max(0, 1 - e^{-2\beta J s_i^x s_j^x})$  [15, 44]. Due to a similar reason as that in the Potts model, the correlation function restricted on the direction  $\hat{x}$  of the XY model is preserved. Therefore the phase transition in the XY model can be inferred from the percolation transition of the correlated percolation model.

For the correlated percolation model generated based on the Potts model and the XY model, the AIM configurations can be obtained by randomly assigning  $\pm 1$  to different clusters. The previous proof also applies here, that, after the AIM transformation, the correlation functions of the correlation percolation model and the Auxiliary Ising spin model are equivalent.

Then the confusion method can be applied to detect the phase transition of the correlated percolation model in an unsupervised way. In Figs. 6 (a) and (b), the performance curves by using the AIM configurations of the  $q = 5$  Potts model and the XY model as training data are shown, respectively. Clear W-shaped performance curves emerge for the Potts model, indicating that the confusion method detects a phase transition. Furthermore, the peak position of the performance curve is consistent with the critical point  $T_c/J = 1/\ln(1 + \sqrt{5}) = 0.852$  [45] within the numerical discrete step  $\Delta T = 0.02J$ .

As for the XY model, W-shaped performance curves also show up at sizes  $L = 60, 80, 100$  and the peaks of the performance curves are about  $T/J \approx 1.04$ , which is approximate to the result obtained by the confusion method without using the AIM transformation [31, 32]. Although the peak position has a tendency to become

closer to the true BKT critical point as the system size increases, we still can not claim a clear relation between the peak and the BKT critical point  $T/J \approx 0.8935(1)$  [46, 47]. We suggest that this slow-converging peak position is probably a result of the logarithmic finite-size correction of stiffness and linear size  $L$  at the BKT phase transition point [47–49]. The deviations from the estimated values of the phase transition points in Refs. [31, 32] probably come from the same reason.

### III. IDENTIFICATION OF UNIVERSALITIES

The study of universality and the critical exponent is an important task in statistical physics [50]. Machine learning, as an emerging approach, has been applied recently to extract universality and critical exponent [51, 52]. In the two dimensional  $q$ -state Potts model, a second-order transition occurs at  $q \leq 4$  and a first-order phase transition for otherwise [53, 54]. For 2-state Potts and other Potts models, the difference in universalities leads to different correlated percolation configurations in FK representation at the phase transition point, respectively. This difference is difficult to distinguish by conventional data analysis methods.

The AIM method is a physics-preserved transformation, therefore the universality and scaling behavior remain unchanged after the mapping. In this section, we demonstrate that the universality differences in different Potts model after the AIM transformation can be detected.

We generate the AIM configurations of the  $q=\{3,4,5,6,7,8,9,10\}$  state Potts models at their respective critical points at different system sizes, which are mixed with the AIM configurations of the 2-state Potts model and fed into the binary classification neural network described in Appendix A 2. The classification results are evaluated by the binary classification accuracy, which is the ratio of the number of correctly predicted samples to the total number of samples and can be expressed as [55]:

$$\text{Accuracy} = \frac{\text{TP} + \text{TN}}{\text{TP} + \text{FP} + \text{TN} + \text{FN}}, \quad (7)$$

where true-positive (TP) is the number of samples for which the model correctly predicts the positive class, and the other three cases true-negative (TN), false-positive (FP) and false-negative (FN) are defined in a similar way.

Figure 7 shows the binary classification accuracy. Two features can be observed: (I), as the Potts number  $q$  increases, the binary classification accuracy increases. This is because the  $q$ -state Potts model tends to have a more drastic phase transition as  $q$  increases. (II), the binary classification accuracy increases as the size of the system increases, which indicates that the features acquired by the neural network are still maintained in the thermodynamic limit.

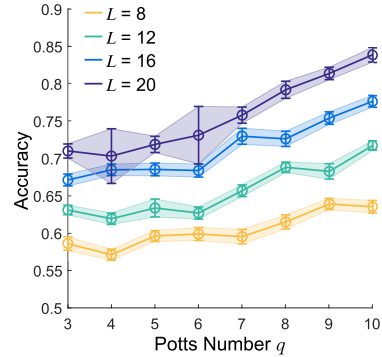


FIG. 7. Binary classification accuracy of 2-state Potts model and other  $q$ -state Potts models at different system sizes. The data input to the neural network are all auxiliary Ising configurations mapped from the  $q$  state Potts model at the respective phase transition points.

In summary, the above results imply that the neural network can distinguish different universalities from the configurations obtained after the AIM transformation.

### IV. SUMMARY AND DISCUSSION

In this paper, we propose the auxiliary Ising mapping method for machine learning to detect both uncorrelated and correlated percolation transition in an unsupervised way. To demonstrate that the robustness of this method, we have validated it under site percolation model, bond percolation model, Potts model, and XY model on different lattices. The results show that the confusion scheme, which failed in the percolation model, could learn the geometric phase transition correctly with our mapping method. For the XY model, the observed deviated peak position probably come from a logarithmic finite-size correction. Furthermore, we also show that the universalities of the Potts model with different values of  $q$  can be distinguished by neural networks with the AIM method.

There are many ways in which the state of a physical system can be represented as a dataset, and applying machine learning to a more feature-specific representation can make machine learning more effective. Auxiliary variables, e.g., the Ising-like spins, can be one of such representations. This approach might advance the application of machine learning in statistical and condensed-matter physics.

### ACKNOWLEDGMENTS

We thank Heyang Ma and Guimin Lin for discussions. Y. D is supported by the National Natural Science Foundation of China (under Grant No. 11625522), the Science and Technology Committee of Shanghai (under grant No. 20DZ2210100), the National Key R&D Program of China (under Grant No. 2018YFA0306501). W. Z is supported

by the open project KQI201 from Key Laboratory of Quantum Information, University of Science and Technology of China, Chinese Academy of Sciences.

### Appendix A: The structure of Network

In both the confusion scheme and the universality classification, we use the binary classification neural networks. The binary classification neural network is designed for the classification of the samples in a supervised way, which is generally composed of three main parts: the input layer, the hidden layer(s), and the output layer. The input layer, which has the same dimension as the input data, can be both a fully connected layer or convolution layer. For the hidden part, there can be more than one layer, and a composed structure can be utilized by combining the convolution layer and the fully connected layers. For the output layer in a binary classification neural network, there are generally two choices: one output form and two output forms, which are equivalent to each other. In our work, we used the previous one. For a binary classification task, all the samples are pre-labeled with 0 or 1, which refer to the two different classes. The samples are then separated into a training set and a test. Gradient descent algorithm is used to train the neural network out of the training set in order to teach the neural network to find the hidden difference within the 0 and 1 data. The loss function we used in binary classification is the binary cross-entropy, which is defined as [55]:

$$L = \frac{1}{N} \sum_i - (y_i \log(p_i) + (1 - y_i) \log(1 - p_i)) , \quad (\text{A1})$$

where  $N$  is the number of the data in the training set,  $y_i$  is the label (0 or 1) for the  $i$ -th sample and  $p_i$  is the output of the output neuron, which refers to the probability that the  $i$ -th sample is predicted with label 1. It can be seen that, by minimizing the binary cross-entropy, the neural network is approaching a better classification out of the training set. To quantify the training result, we further apply the neural network we trained onto the test set and give the predicted label  $y'_i$  for the  $i$ -th sample according to the output neural: if the output is larger than 0.5, then  $y'_i = 1$ , otherwise,  $y'_i = 0$ . We quantify the performance of the classification network by the binary classification accuracy defined in Eq.( 7). In the confusion scheme, the binary classification accuracy obtained by training the network using trial labels is called the confusion performance.

### 1. Binary Classification for Confusion Scheme

The structure of this neural network is shown in Fig. 1. The neural network we use has one input layer, one hidden layer, 10 neurons in the hidden layer, and the ReLu

function is chosen as the activation function. An L2-regularization with a rate of 0.001 to avoid over-fitting. The output neuron uses Sigmoid as the activation function to obtain the output in the interval  $[0, 1]$  to indicate the classification accuracy. We randomly select 40,000 samples out of 60,000 as the training set and the rest as the test set in each confusion training. In the training process, we set the batch size of the training set to 512, use the RmsProp algorithm for adaptive gradient descent training, train epoch to 30, and finally use the cross-entropy as the loss function.

### 2. Binary Classification for universality Classification

The structure of the binary classification network used to classify different universalities of Potts model is shown in Fig. 8. The first two layers are convolution networks, the kernel size is  $3 \times 3$ , the first layer has 32 channels while the second layer has 16 channels. A fully connected layer with ten neurons is placed behind the convolutional layer. Rectified linear unit (ReLu) is chosen as the activation functions for the first three layers. The output neuron is activated by Sigmoid function. In order to avoid overfitting, L2 regularization is used in the third layer (fully connected layer with 10 neurons), the L2 regularization rate is 0.001.

To obtain the data used in Fig. 7, the training set consists of 8000 samples, while the test set has 2000 samples. The number of training epoch is 10, and the batchsize is chosen to be 32 in each epoch.

### Appendix B: Confusion scheme

The confusion scheme is invented to detect phase transition and locates the phase transition point without knowing any prior knowledge of the phases. The main technique used in the confusion scheme is the use of trial labels. For a phase transition controlled by one variable, such as the 2D Ising model without external magnetic fields controlled by temperature  $T$ , the configurations can be classified into two different classes: the ferromagnetic phase  $T < T_c$  and the disorder phase  $T > T_c$ . Therefore, if we have to separate the data with different  $T$  into two classes, the separation according to  $T_c$  will result in the maximum differences between the two classes, therefore generally leads to a higher binary classification accuracy obtained by the neural network. The main idea of the confusion scheme is to find such accuracy peaks, or rather, performance peaks, which help to detect phase transitions and assign transition points. The algorithm for the confusion scheme is shown as the following:

(1) Prepare a dataset for machine learning. Taking the site-percolation model as an example, we divide the parameter range  $[p_{min}, p_{max}]$  into  $N_p$  parameters  $\{p_i\}$  and generate  $N_s$  samples of both the original configurations

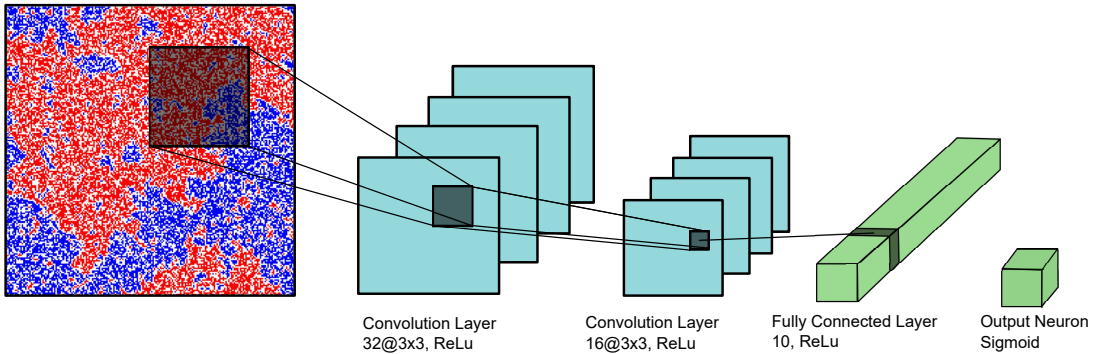


FIG. 8. The structure of the binary classification network is used to classify the different universalities of the Potts model. Layer One: Convolutionlayer, 32 channels, the kernel size is  $3 \times 3$ , activated by ReLu. Layer Two: Convolution layer, 16 channels, the kernel size is  $3 \times 3$ , activated by ReLu. Layer Three: Fully connected layer, 10 neurons, activated by ReLu. Output layer: one output neuron activated by Sigmoid function.

and the auxiliary Ising spin configurations at each parameter  $p_i$ . This gives us  $N = N_p \times N_s$  configurations.

(2) Make the trial labels and perform training and testing. The  $p_i$  is chosen as the trial critical point for generating trial labels, and all samples generated with  $p_j < p_i$  are assigned label 0, and the rest are assigned label 1. A binary classification neural network is then trained to classify the samples while recording the accuracy  $Acc(p_i)$  or called performance.

(3) Repeat step 2 with all trial critical points  $\{p_i\}$  in the range  $[p_{min}, p_{max}]$ , and obtain the performance curve.

For the trial critical locates at the lower (or upper) boundary for the parameter regime, all trial labels are 0 (or 1), which will result in a perfect classification with 100% accuracy. Therefore, if there are no phase transitions in the parameter investigated parameter range or the difference between two phases is still too difficult for the neural network to capture, then a V-shaped performance curve can be expected.

From the reasoning above, we also know that the local maximum of performance will be obtained if the trial

labels exactly refer to different phases. In that case, the performance curve would have several local maxima that separate different phases, therefore, allocate the phase transition point. For a special case that the system has only two distinguished phases, such as the site percolation model on the square lattice, then the performance curve would be a W-shaped curve, and the peak locates exactly at the phase transition point.

### Appendix C: ER network

Erdős–Rényi model is initially proposed by Paul Erdős and Alfréd Rényi for generating random graphs [38].

The ER network consists of  $N$  isolated vertices and  $rN$  edges are added randomly to connect those vertices. Varying the percolation parameter  $r$ , the system undergoes a second-order phase transition at  $r = r_c = 1/2$ . For  $r < r_c$ , the ER network is disjoint with small clusters; for  $r > r_c$ , the percolated cluster emerges.

---

[1] S. R. Broadbent and J. M. Hammersley, Percolation processes: I. Crystals and mazes, in *Math. Proc. Camb. Philos. Soc.*, Vol. 53 (Cambridge University Press, 1957) pp. 629–641.

[2] A. Hunt, R. Ewing, and B. Ghanbarian, *Percolation theory for flow in porous media*, Vol. 880 (Springer, 2014).

[3] M. E. J. Newman, Spread of epidemic disease on networks, *Phys. Rev. E* **66**, 16128 (2002).

[4] D. Duffie and G. Manso, Information percolation in large markets, *Am. Econ. Rev.* **97**, 203 (2007).

[5] M. V. Men'shikov, S. A. Molchanov, and A. F. Sidorenko, Percolation theory and some applications, *J. Sov. Math.* **42**, 1766 (1988).

[6] R. Cohen, K. Erez, S. Havlin, M. Newman, A.-L. Barabási, and D. J. Watts, Resilience of the internet to random breakdowns, in *The Structure and Dynamics of Networks* (Princeton University Press, 2011) pp. 507–509.

[7] D. S. Callaway, M. E. J. Newman, S. H. Strogatz, and D. J. Watts, Network robustness and fragility: Percolation on random graphs, *Phys. Rev. Lett.* **85**, 5468 (2000).

[8] D. Achlioptas, R. M. D'Souza, and J. Spencer, Explosive percolation in random networks, *Science* **323**, 1453 (2009).

[9] M. Li, R.-R. Liu, L. Lü, M.-B. Hu, S. Xu, and Y.-C. Zhang, Percolation on complex networks: Theory and application, *Phys. Rep.* **907**, 1 (2021).

[10] C. M. Fortuin and P. W. Kasteleyn, On the random-cluster model: I. Introduction and relation to other models, *Physica* **57**, 536 (1972).

[11] C. Fortuin, On the random-cluster model ii. the percolation model, *Physica* **58**, 393 (1972).

[12] M. E. Fisher, Magnetic critical point exponents—their interrelations and meaning, *J. Appl. Phys.* **38**, 981 (1967).

[13] A. Coniglio and W. Klein, Clusters and Ising critical droplets: a renormalisation group approach, *J. Phys. A Math. Theor.* **13**, 2775 (1980).

[14] C.-K. Hu, Percolation, clusters, and phase transitions in spin models, *Phys. Rev. B* **29**, 5103 (1984).

[15] R. H. Swendsen and J.-S. Wang, Nonuniversal critical dynamics in Monte Carlo simulations, *Phys. Rev. Lett.* **58**, 86 (1987).

[16] G. Carleo, I. Cirac, K. Cranmer, L. Daudet, M. Schuld, N. Tishby, L. Vogt-Maranto, and L. Zdeborová, Machine learning and the physical sciences, *Rev. Mod. Phys.* **91**, 045002 (2019).

[17] L. Wang, Discovering phase transitions with unsupervised learning, *Phys. Rev. B* **94**, 195105 (2016).

[18] S. J. Wetzel, Unsupervised learning of phase transitions: From principal component analysis to variational autoencoders, *Phys. Rev. E* **96**, 022140 (2017).

[19] W. Hu, R. R. P. Singh, and R. T. Scalettar, Discovering phases, phase transitions, and crossovers through unsupervised machine learning: A critical examination, *Phys. Rev. E* **95**, 062122 (2017).

[20] W. Zhang, J. Liu, and T.-C. Wei, Machine learning of phase transitions in the percolation and XY models, *Phys. Rev. E* **99**, 032142 (2019).

[21] K. Ch'ng, N. Vazquez, and E. Khatami, Unsupervised machine learning account of magnetic transitions in the Hubbard model, *Phys. Rev. E* **97**, 013306 (2018).

[22] Y. Yang, Z.-Z. Sun, S.-J. Ran, and G. Su, Visualizing quantum phases and identifying quantum phase transitions by nonlinear dimensional reduction, *Phys. Rev. B* **103**, 075106 (2021).

[23] J. F. Rodriguez-Nieva and M. S. Scheurer, Identifying topological order through unsupervised machine learning, *Nat. Phys.* **15**, 790 (2019).

[24] M. S. Scheurer and R.-J. Slager, Unsupervised machine learning and band topology, *Phys. Rev. Lett.* **124**, 226401 (2020).

[25] A. Lidiak and Z. Gong, Unsupervised machine learning of quantum phase transitions using diffusion maps, *Phys. Rev. Lett.* **125**, 225701 (2020).

[26] Y. Long, J. Ren, and H. Chen, Unsupervised manifold clustering of topological phononics, *Phys. Rev. Lett.* **124**, 185501 (2020).

[27] E. P. L. Van Nieuwenburg, Y.-H. Liu, and S. D. Huber, Learning phase transitions by confusion, *Nat. Phys.* **13**, 435 (2017).

[28] S. Cheng, F. He, H. Zhang, K.-D. Zhu, and Y. Shi, Machine learning percolation model, *arXiv preprint arXiv:2101.08928* (2021).

[29] R. Xu, W. Fu, and H. Zhao, A new strategy in applying the learning machine to study phase transitions, *arXiv preprint arXiv:1901.00774* (2019).

[30] J. Wang, W. Zhang, T. Hua, and T.-C. Wei, Unsupervised learning of topological phase transitions using the Calinski-Harabaz index, *Phys. Rev. Research* **3**, 013074 (2021).

[31] P. Suchsland and S. Wessel, Parameter diagnostics of phases and phase transition learning by neural networks, *Phys. Rev. B* **97**, 174435 (2018).

[32] S. S. Lee and B. J. Kim, Confusion scheme in machine learning detects double phase transitions and quasi-long-range order, *Phys. Rev. E* **99**, 43308 (2019).

[33] J. L. Jacobsen, Critical points of potts and O(N) models from eigenvalue identities in periodic Temperley–Lieb algebras, *J. Phys. A Math. Theor.* **48**, 454003 (2015).

[34] X. Feng, Y. Deng, and H. W. J. Blöte, Percolation transitions in two dimensions, *Phys. Rev. E* **78**, 031136 (2008).

[35] M. F. Sykes and J. W. Essam, Exact critical percolation probabilities for site and bond problems in two dimensions, *J. Math. Phys.* **5**, 1117 (1964).

[36] J. L. Jacobsen, High-precision percolation thresholds and Potts-model critical manifolds from graph polynomials, *J. Phys. A Math. Theor.* **47**, 135001 (2014).

[37] H. Kesten, The critical probability of bond percolation on the square lattice equals 1/2, *Commun. Math. Phys.* **74**, 41 (1980).

[38] P. Erdos and A. Rényi, On the evolution of random graphs, *Publ. Math. Inst. Hung. Acad. Sci* **5**, 17 (1960).

[39] K. Malarz and S. Galam, Square-lattice site percolation at increasing ranges of neighbor bonds, *Phys. Rev. E* **71**, 16125 (2005).

[40] M. Majewski and K. Malarz, Square lattice site percolation thresholds for complex neighbourhoods, *Acta Phys. Pol. B* **38** (2007).

[41] D.-R. Tan, C.-D. Li, W.-P. Zhu, and F.-J. Jiang, A comprehensive neural networks study of the phase transitions of Potts model, *New J. Phys.* **22**, 063016 (2020).

[42] C.-D. Li, D.-R. Tan, and F.-J. Jiang, Applications of neural networks to the studies of phase transitions of two-dimensional Potts models, *Ann. Phys.* **391**, 312 (2018).

[43] K. Shiina, H. Mori, Y. Okabe, and H. K. Lee, Machine-learning studies on spin models, *Sci. Rep.* **10**, 1 (2020).

[44] H. Hu, Y. Deng, and H. W. J. Blöte, Berezinskii-Kosterlitz-Thouless-like percolation transitions in the two-dimensional XY model, *Phys. Rev. E* **83**, 011124 (2011).

[45] A. Hintermann, H. Kunz, and F. Y. Wu, Exact results for the Potts model in two dimensions, *J. Stat. Phys.* **19**, 623 (1978).

[46] J. M. Kosterlitz and D. J. Thouless, Ordering, metastability and phase transitions in two-dimensional systems, *J. Phys. C* **6**, 1181 (1973).

[47] Y.-D. Hsieh, Y.-J. Kao, and A. W. Sandvik, Finite-size scaling method for the Berezinskii–Kosterlitz–Thouless transition, *J. Stat. Mech.* **2013**, P09001 (2013).

[48] J. M. Kosterlitz, The critical properties of the two-dimensional xy model, *J. Phys. C* **7**, 1046 (1974).

[49] H. Weber and P. Minnhagen, Monte carlo determination of the critical temperature for the two-dimensional xy model, *Phys. Rev. B* **37**, 5986 (1988).

[50] M. E. Fisher, Renormalization group theory: Its basis and formulation in statistical physics, *Rev. Mod. Phys.* **70**, 653 (1998).

[51] Z. Li, M. Luo, and X. Wan, Extracting critical exponents by finite-size scaling with convolutional neural networks, *Phys. Rev. B* **99**, 75418 (2019).

[52] C. Giannetti, B. Lucini, and D. Vadacchino, Machine learning as a universal tool for quantitative investigations of phase transitions, *Nucl. Phys. B* **944**, 114639 (2019).

[53] R. J. Baxter, Potts model at the critical temperature, *J. Phys. C* **6**, L445 (1973).

[54] R. J. Baxter, H. N. V. Temperley, S. E. Ashley, and S. Edwards, Triangular Potts model at its transition temperature, and related models, *Proc. Math. Phys. Sci.* **358**, 535 (1978).

[55] I. Goodfellow, Y. Bengio, and A. Courville, *Deep learning* (MIT press, 2016).